Intraflagellar transport proteins cycle between the flagellum and its base

Johanna Buisson[1], Nicolas Chenouard[2], Thibault Lagache[2], Thierry Blisnick[1], Jean-Christophe Olivo-Marin[2] and Philippe Bastin[1],*

[1]Trypanosome Cell Biology Unit, Institut Pasteur and CNRS URA2581, 25 rue du Docteur Roux, 75015 Paris, France
[2]Quantitative Image Analysis Unit, Institut Pasteur and CNRS URA2582, 25 rue du Docteur Roux, 75015 Paris, France
*Author for correspondence (philippe.bastin@pasteur.fr)

Journal of Cell Science

Summary

Intraflagellar transport (IFT) is necessary for the construction of cilia and flagella. IFT proteins are concentrated at the base of the flagellum but little is known about the actual role of this pool of proteins. Here, IFT was investigated in *Trypanosoma brucei*, an attractive model for flagellum studies, using GFP fusions with IFT52 or the IFT dynein heavy chain DHC2.1. Tracking analysis by a curvelet method allowing automated separation of forward and return transport demonstrated a uniform speed for retrograde IFT (5 µm s^{-1}) but two distinct populations for anterograde movement that are sensitive to temperature. When they reach the distal tip, anterograde trains are split into three and converted to retrograde trains. When a fast anterograde train catches up with a slow one, it is almost twice as likely to fuse with it rather than to overtake it, implying that these trains travel on a restricted set of microtubules. Using photobleaching experiments, we show for the first time that IFT proteins coming back from the flagellum are mixed with those present at the flagellum base and can reiterate a full IFT cycle in the flagellum. This recycling is dependent on flagellum length and IFT velocities. Mathematical modelling integrating all parameters actually reveals the existence of two pools of IFT proteins at the flagellum base, but only one is actively engaged in IFT.

Key words: Intraflagellar transport, Cilia and flagella, Trypanosome

Introduction

The construction of cilia and flagella relies on the bi-directional movement of protein complexes (IFT particles or trains) called intraflagellar transport (IFT), a process that was discovered in the green alga *Chlamydomonas reinhardtii* (Kozminski et al., 1993). IFT is driven by motors of the kinesin II family in the anterograde direction (from base to tip) (Kozminski et al., 1995) and by a specialised dynein complex in the retrograde orientation (Rompolas et al., 2007). IFT particles are visualised by transmission electron microscopy as electron-dense granules positioned between the flagellum membrane and the axoneme peripheral microtubules (Kozminski et al., 1995; Absalon et al., 2008; Pigino et al., 2009). They were purified from *Chlamydomonas* flagella and shown to contain two protein complexes termed A and B (Cole et al., 1998). Genes encoding motors or IFT proteins are conserved in most ciliated eukaryotic species (Hao and Scholey, 2009) and inhibition of IFT motor or particle components perturbs construction of the organelle in all species investigated so far, from protists to mammals (Kozminski et al., 1995; Brown et al., 1999; Signor et al., 1999; Pazour et al., 2000; Huangfu et al., 2003; Kohl et al., 2003).

So far, IFT has been demonstrated by differential interfering contrast microscopy in live cells as the movement of particles deforming the flagellum membrane (only in *Chlamydomonas*) (Kozminski et al., 1993) or by monitoring individual IFT components fused to a fluorescent protein (Orozco et al., 1999). However, these observations are limited to few cell types (Follit et al., 2006; Absalon et al., 2008; Tran et al., 2008) and detailed investigation is only available for *Chlamydomonas*

(Dentler, 2005) and for different types of ciliated neurons in *C. elegans* where unexpected differences have been reported (Snow et al., 2004; Morsci and Barr, 2011). Imaging IFT in mammals has been challenging and data have only been reported for the primary cilium of LLC-PK1 and IMCD cultured cells (Follit et al., 2006; Besschetnova et al., 2009). These studies revealed quite significant differences in IFT rates and in the nature of IFT anterograde motors and highlight the importance for further investigation in distinct cellular contexts.

The protist *Trypanosoma brucei* is an attractive model to study IFT as it possesses a long flagellum (20 µm) with a typical axonemal structure and is amenable to potent reverse genetics. Genomic and functional analysis demonstrated the conservation of almost all *IFT* genes (Julkowska and Bastin, 2009). We reported the first visualisation of IFT in trypanosomes by monitoring movement of IFT52 (a member of the IFT-B complex) fused to GFP (Absalon et al., 2008). We have now set up appropriate conditions to image IFT and have developed a software to detect and track IFT particles upon kymograph analysis, allowing semi-automatic analysis and easy discrimination of anterograde and retrograde traffic, significantly improving the signal-to-noise ratio (Chenouard et al., 2010). This opened up the possibility to investigate some of the multiple key aspects in IFT mechanistic that remain unsolved, such as for example the selection of the doublet microtubule on which trains are going to travel. We show here the existence of at least two distinct anterograde populations travelling with different speed in the same portion of the flagellum. Remarkably, fusion events were almost twice more likely to

happen than overtaking cases, supporting the view that anterograde trains travel on a limited number of microtubule doublets. We also show that anterograde trains are split in three once they reach the distal tip, solving a conundrum between train size and frequency of anterograde and retrograde transport from other studies (Pigino et al., 2009). Finally, photobleaching experiments demonstrate for the first time the recycling of IFT proteins returning from the flagellum to the flagellum base and mathematical modelling revealed that only ~45% of the basal pool is actively engaged in IFT.

Results

Detection and tracking of fluorescent IFT particles

IFT was visualised in live procyclic trypanosomes (those that normally develop in the fly midgut) expressing the IFT complex B component IFT52 fused to GFP (Absalon et al., 2008). GFP::IFT52 was found in high concentration at the flagellum base, as elongated spots in the flagellum and present uniformly in the cell body with the exception of the nucleus (Fig. 1). Images were acquired upon immobilisation in an agarose matrix using movie recording. However, the signal-to-noise ratio in the flagellum was low and retrograde events extremely difficult to detect. We therefore improved viewing and acquisition conditions. First, we noticed that cells frequently stick to glass slides with their flagellum lying on the side, allowing visualisation of long segments of the organelle in a single z-plane (Fig. 1). Second, we used digital recording with a CCD camera to detect IFT trains in the flagellum. A 150 ms exposure provided clear and unambiguous detection of anterograde events

that appear as elongated traces (Fig. 1A; supplementary material Movie 1), but retrograde events remained difficult to detect. When visible, they appeared as very elongated traces of weak intensity that could not be tracked accurately.

To improve sensitivity, GFP::IFT52 expressing trypanosomes were observed under laser illumination using the spinning disk technology and images were acquired with an amplified EMCCD camera (Fig. 1B,C; supplementary material Movies 2, 3). This allowed reduction of the exposure time to 100 ms and both anterograde and retrograde particles then appeared as defined spots whose path could be followed along the whole length of the flagellum (colour arrows on still images at Fig. 1B,C). To ensure that these were not restricted to IFT52, we constructed a fusion between the genes encoding GFP and the IFT dynein heavy chain (DHC2.1, also called DHC1b), the motor for retrograde transport. Anterograde and retrograde IFT events were observed for GFP::DHC2.1 (Fig. 1D; supplementary material Movie 4), as well as for five distinct components of the IFT machinery (two IFTB proteins -IFT22 and IFT27- and three subunits of the dynein complex DHC2.2, XBX1 and FAP133, our unpublished data). In contrast, IFT was not observed when GFP was fused to structural flagellar proteins such as DNAI1, an intermediate chain of the outer dynein arm or PFR2, one of the main components of the paraflagellar rod, a large structure found alongside the axoneme (our unpublished data).

Kymograph analysis was next carried out on cells filmed for 30 s where the position of the particle is marked on the x-axis and time is projected on the y-axis (Fig. 2A,B; supplementary material Movie 5). However, bi-directional IFT yields many
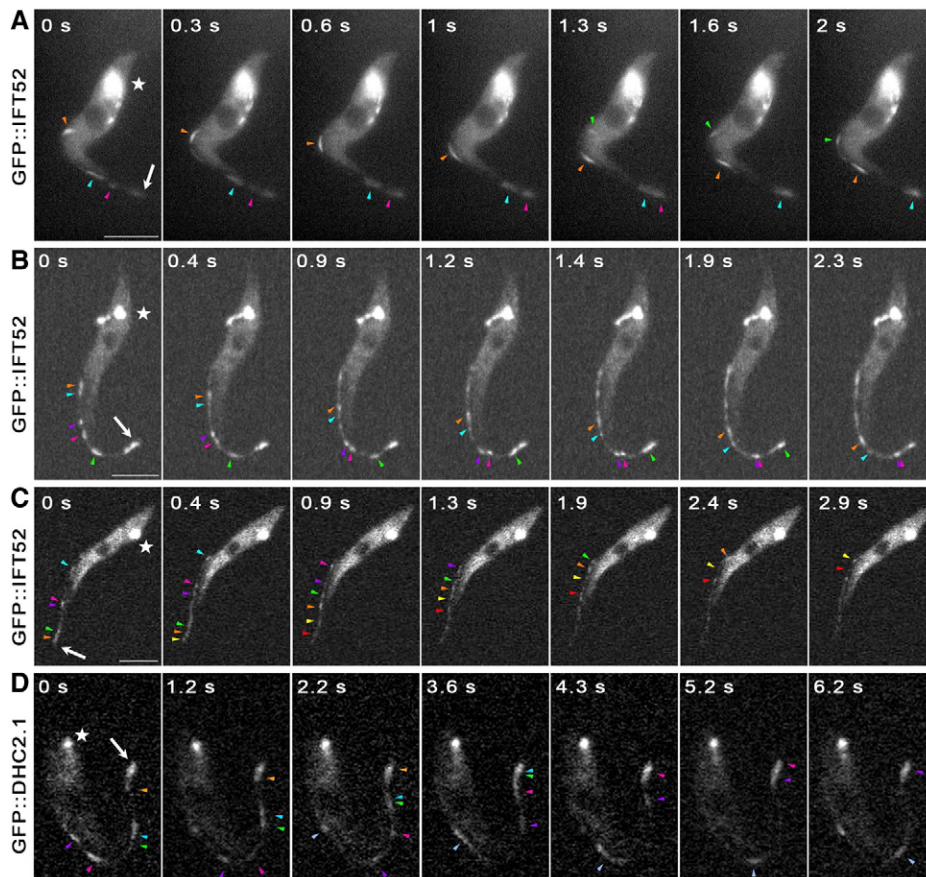

Fig. 1. Anterograde and retrograde intraflagellar movement of EGFP::IFT52 and EGFP::DHC2.1. Each row shows still images from movies of cells expressing GFP::IFT52 (A–C, supplementary material Movies 1–3) or GFP::DHC2.1 (D, supplementary material Movie 4) as indicated. The successive position of anterograde (A,B,D) and retrograde (C) trains on each image is indicated by coloured arrowheads. On the first image on the left, the white star indicates the position of the flagellum base and the white arrow marks the distal end of the flagellum. (A) Cells were illuminated on a conventional epifluorescence microscope and images were acquired with a 150 ms exposure using a CCD camera. (B–D) Fluorescence was excited with a laser using a microscope equipped with a spinning disk and images acquired with a 100 ms exposure using an EMCCD camera. (B) Movement of anterograde trains. (C) To visualise retrograde trains that are regularly masked by larger anterograde particles, the flagellum base was photo-bleached to prevent entry of new fluorescent trains. Once all the fluorescent anterograde trains reached the tip of the flagellum, only retrograde trains are visible (see Fig. 5 and text). (D) IFT movement of GFP::DHC2.1. Scale bars: 5 μm.
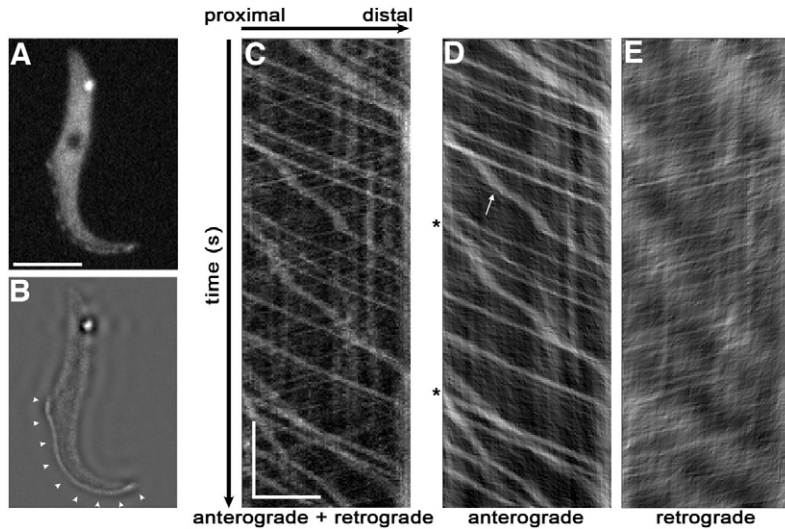
Fig. 2. Kymograph generation and separation of anterograde and retrograde traces. (**A**) Still image of supplementary material Movie 5 from which the kymograph was extracted. (**B**) The visible portion of the flagellum used for analysis is highlighted (arrowheads). Scale bar: 5 μm for both images. (**C**) Kymograph extracted from supplementary material Movie 5 where the X axis corresponds to the length of the flagellum (horizontal scale bar, 5 μm) and the Y axis to the elapsed time (vertical scale bar: 5 s). Anterograde (**D**) and retrograde (**E**) traces have been separated hence reducing background and allowing for straightforward analysis (same magnification as C). Arrows indicate some slow trains that changed speed during their trip in the flagellum and stars point at very slow trains.

cross-points in the kymograph image, which prevents using a simple automatic procedure for IFT quantification. We therefore developed a kymograph analysis technique based on a curvelet transform that permits the separation of anterograde and retrograde IFT particles in two distinct sub-kymograph images (Chenouard et al., 2010). As a result, crossing points between bi-directional trails are no longer present, which greatly improves the analysis of retrograde trains usually masked by the larger and brighter anterograde particles (Fig. 2C,D, see below). To increase the number of cells amenable for analysis, successive movies of separate trypanosomes maintained in medium on the same slide were acquired. Measurement of both anterograde and retrograde velocities showed that these parameters were unaltered over a period of acquisition of up to an hour (supplementary material Fig. S1). Overall, the acquisition conditions and the automatic analysis of kymographs allow robust and reproducible analysis of both IFT anterograde and retrograde events in the trypanosome flagellum.

Quantification of IFT speed and frequency

Kymograph analysis of anterograde events demonstrated an unexpected complexity, with trains exhibiting highly dissimilar rates within the same flagellum (Figs 2, 3). Examination of train speed suggested the existence of at least two peaks. The hypothesis was tested using a Bayesian information criterion (BIC) (Schwarz, 1978) (see Materials and Methods) that showed a bimodal distribution of anterograde trains in most individual sequences (71% of 41 films) for both GFP::IFT52 and GFP::DHC2.1 (Fig. 3A,B, dark grey bars). About 67% of the trains showed fast motility (2.40 ± 0.31 μm s^{-1}, $n=551$, Table 1) whereas ~33% of them displayed slower motion (1.53 ± 0.30 μm s^{-1}, $n=271$, Table 1). Moreover, we noticed the presence of a minor population of trains travelling at very slow speed (stars, Fig. 2D). Their proportion was too low to be detected in a significant statistical analysis but they were consistently detected on many movies. They represent 4.7% of the total number of anterograde trains for GFP::IFT52 ($n=1,223$) and 5.9% in the case of GFP::DHC2.1 ($n=442$), with a speed of 0.55 ± 0.24 μm s^{-1}, and 0.52 ± 0.30 μm s^{-1}, respectively.

Examination of complete traces from the base to the tip of the flagellum revealed that trains displayed fast or slow motions as

soon as they could be detected in the flagellar compartment (Fig. 2D). However, whereas most fast trains maintained the same speed for the complete anterograde journey, slow trains frequently showed modification of their motion during their trip along the flagellum (Fig. 2D, arrows). Fast and slow trains actually interact in the flagellum, leading to more complex events (see below). In contrast, retrograde transport appeared more homogenous, as evidenced on the kymographs where traces were mostly parallel to each other (Fig. 2E, Fig. 3A–C). Accordingly, the BIC indicated that a single Gaussian model was the best fitting model for retrograde transport in every movie, uncovering the fastest IFT motion reported so far: 5.64 ± 1.01 μm s^{-1} ($n=1,223$) (Fig. 3A,B, light grey).

The frequency of visible IFT trains was calculated at both the proximal and the distal end of the flagellum, revealing an almost 3-fold higher abundance of retrograde events compared to anterograde ones (Table 2). Calculation of IFT train intensity was performed along their entire visible path and showed that anterograde trains carry on average ~4.1-fold more IFT52 material than their retrograde counterparts. The length of the traces left by the anterograde train was 393 ± 51 nm ($n=505$, from 10 separate movies using kymograph analysis) whereas that of the retrograde train was 250 nm± 51 nm ($n=539$, from 10 separate movies using kymograph analysis). These have to be taken as approximations given the limitations imposed by the acquisition time (100 ms), the speed of the trains and the resolution of light microscopy.

IFT is sensitive to temperature

Trypanosomes develop in two different hosts, where they encounter very different environmental conditions, such as varying temperatures during fly infection, a main contributor to differentiation (Engstler and Boshart, 2004). Procyclic trypanosomes were grown at 27°C as usual and then incubated in a chamber where temperature could be controlled accurately and rapidly. Increasing the observation temperature to 37°C did not affect the occurrence of two distinct velocities for anterograde transport and only one for retrograde transport, a feature that was supported by the BIC analysis (Fig. 3C; supplementary material Movie 8). However, it resulted in accelerated IFT speed for all train categories, with a 1.4-fold
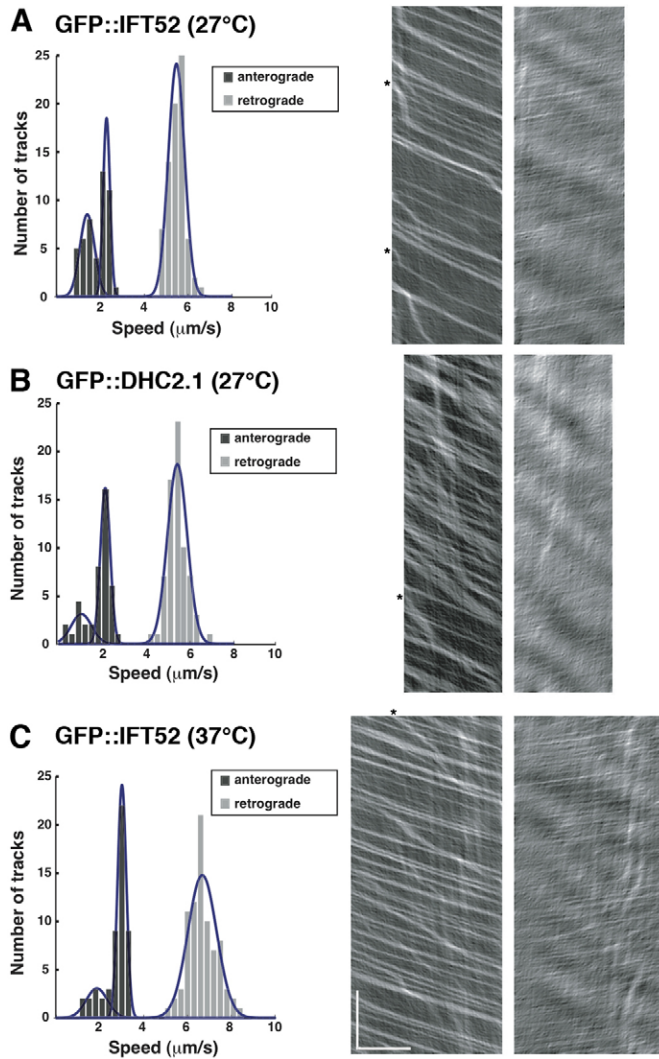
Fig. 3. **Anterograde and retrograde IFT and sensitivity to temperature.** (**A–C**). Speed of anterograde (dark grey) and retrograde (light grey) IFT trains in the indicated cell lines exposed to 27℃ (A,B; still images from supplementary material Movies 6 and 7, respectively) or 37℃ (C; still image from supplementary material Movie 8). BIC analysis detected two separate populations of trains for anterograde transport whereas only one can be identified for retrograde transport. The obtained Gaussians for each anterograde population are represented as blue lines. All populations travel faster when cells are incubated at 37℃ (C). Stars point at some very slow trains. All kymographs are shown at the same magnification. Scale bars: horizontal, 5 µm; vertical, 5 s.

increase for slow anterograde trains and a 1.3-fold increase for the fast ones. Trains displaying slower velocity were still detected in similar proportion than at 27℃ (5.6% of the anterograde trains, $n=707$) but had a faster velocity at 1.07 ± 0.23 µm s^{-1} (Fig. 3C, star). Finally, a similar 1.37-fold increase was noticed for retrograde transport reaching a spectacular average velocity of 7.42 ± 1.64 µm s^{-1} ($n=742$) (Table 1). This acceleration of IFT velocities was accompanied by an increase in the frequency of trains that was slightly more pronounced for retrograde events (Table 2). In contrast, reducing the temperature to 20℃ did not lead to visible modifications of IFT speed (data not shown). To our knowledge, this is the first demonstration of an effect of

temperature on IFT velocity, a phenomenon that could have significant consequences for ciliated cells exposed to variable temperatures.

Anterograde trains interact within the same flagellum
The existence of populations displaying different anterograde motions in the same flagellum implies that fast particles should catch up with slow ones, providing a way to evaluate whether anterograde trains travel on the same or on distinct microtubule doublets. This gives rise to three types of events that were all detected in kymographs (Fig. 4). First, a fast train could overtake one (Fig. 4A) or more (Fig. 4A′) slow trains without modification of their initial speed. Such events were frequently detected in most movies, with the most common situation being the case of a slow IFT train that was overtaken by one or two fast trains, and on a few occasions by 3 (Fig. 4A′) or more fast trains (Fig. 4D). This was not accompanied by a visible temporary deceleration or arrest of the fast train at the passing point, as confirmed by the continuity of the anterograde traces on the kymograph (Fig. 4A). This suggests that these trains travel independently, presumably on separate microtubule doublets. A second type of situation was observed when a fast train caught up a slow one and apparently fused with it, leading to either unchanged speed (the fast one 'pushes' the slow one, Fig. 4B) or reduced speed (the slow one 'slows down' the fast one, Fig. 4B′). Fusion events turned out to be very frequent (Fig. 4D), with a clear predominance of fast particles maintaining their initial speed (102 events out of 117, pink colour on Fig. 4D). Such fusion events imply that both trains travel on the same or closely positioned doublet microtubules. Their proportion relative to the overtaking events was 1.4-fold higher.

Finally, fission events were also observed when a fast train left a slow one behind (Fig. 4C), or alternatively when a slow train let a fast one 'escape' (Fig. 4C′). There was a strong bias in favour of the first situation (77 out of 92 events, pink colour on Fig. 4D). These results indicate that slow and fast trains actively interact within the flagellum. They imply that train frequency could change during the trip to the flagellum and we therefore compared it between the proximal and distal ends of the flagellum (Table 2). This revealed a slight decrease in train frequency at the distal end, in agreement with the higher proportion of fusion events relative to the fission events (1.2:1 ratio). In contrast, the frequency of retrograde transport was unchanged, in agreement with the absence of detectable fusion or fission events.

IFT proteins actively exchange between the flagellum base and the flagellum compartment
The contribution of the pool of IFT proteins concentrated at the flagellum base to IFT taking place in the flagellum is unknown. To address this pool, FRAP analysis was performed. First, it was confirmed that such an exposure did not affect IFT. Indeed, the measured anterograde and retrograde IFT rates after bleaching were equivalent to non-exposed cells (data not shown). Next, appropriate conditions were set up to normalise data for overall photobleaching due to laser exposure and to quantify fluorescent signals, taking into account the high differences in local signal intensities (see Materials and Methods). This is really challenging since non-ambiguous detection of IFT trains in the flagellum requires a 100 ms exposure that usually results in saturation of

Table 1. IFT velocities of anterograde and retrograde trains

| Strain | T | n | Anterograde trains | | Retrograde trains | |
			Slow speed	Fast speed	n	Speed
IFT52	27°C	822	1.53±0.30	2.40±0.31	1223	5.64±1.01
DHC2.1	27°C	191	1.34±0.20	2.25±0.14	210	4.99±0.89
IFT52	37°C	528	2.22±0.37	3.21±0.46	742	7.42±1.64

Rates are given in µm s^{-1}. Slow and fast anterograde trains were separated by the BIC.

the flagellum base signal, rendering quantification of the fluorescence recovery impossible. Nevertheless, screening through a large number of cells allowed the identification of a few of them in which the GFP::IFT52 signal at the flagellum base was not saturated in acquisition conditions where the trains were detectable in the flagellum. GFP fluorescence at the flagellum base of such cells was selectively bleached and recovery was evaluated by quantifying intensity at the flagellum base, by examining overall fluorescence distribution and by performing kymograph analysis to monitor fluorescent trains in the flagellum.

Two movies are presented: supplementary material Movie 9, where fluorescence intensity is saturating at the flagellum base but allows easy visualisation of the different IFT trains in the flagellum (Fig. 5A) and supplementary material Movie 10 where the signal is weaker but non-saturating, permitting reliable quantification of fluorescence intensity at the flagellum base (Fig. 5B). In both cases, bleaching was achieved by a single laser pulse, leading also to disappearance of the fluorescent cytoplasmic signal in close vicinity of the flagellum base (Fig. 5Ac). This resulted in the almost immediate loss of new fluorescent anterograde trains in the flagellum. By contrast, both anterograde and retrograde trains present in the flagellum before bleaching retained their fluorescence intensity and kept on moving at their usual rates (Fig. 5Ad). The first sign of recovery was observed less than 1 s later when the cytoplasmic area surrounding the flagellum base was replenished, indicating rapid dynamics of the cytoplasmic pool of GFP::IFT52 (Fig. 5Ad). Meanwhile, the flagellum contained a mixture of anterograde and retrograde trains for ~10–15 s after bleaching (Fig. 5Ae) until the last anterograde fluorescent particle reached the distal tip of the flagellum (green arrowheads, Fig. 5Af). From that moment on, exclusively retrograde fluorescent particles were detected (violet arrowheads, Fig. 5Ag) until 4 s later where anterograde fluorescent trains were again visible (Fig. 5Ah). Their intensity was weaker compared to the original trains but they displayed the same diversity of fast and slow particles as unbleached cells (Fig. 5Aa). Once these particles reached the distal tip, they were converted to retrograde trains, leading to the typical IFT pattern with anterograde and retrograde trains, although with reduced intensity (Fig. 5Ai).

Recovery data of the GFP::IFT52 signal at the flagellum base were averaged from 10 separate films and are presented at Fig. 5B. Rapid and steady recovery is observed immediately after photobleaching until a plateau is reached (Fig. 5B). This was achieved after 20–24 s and reached 46±8% of the original value. If one considers that the recovery of fluorescent proteins at the flagellum base is due to material coming back from the flagellum, this can be calculated by integrating all IFT parameters described above in a transport model (Fig. 5C). From the frequency analysis, we know that an anterograde train contains three times more material than a retrograde one. This one was therefore defined as the basic unit (green rectangles, Fig. 5B). To calculate the number of IFT units present in the flagellum, we first measured the time spent for a full cycle by taking into consideration the length of the flagellum (22.3 µm) (Robinson et al., 1995) divided by the average velocity of anterograde (0.66*2.4+0.33*1.5 µm s^{-1}, so ~11 s) and retrograde trains (5.6 µm s^{-1}, so ~3.5 s). With a frequency of 0.9 trains (or 2.7 units) per second, we can deduce that at any given time, ~9 anterograde trains (six fast and three slow ones, total of 27 units) and ~10 retrograde trains are trafficking in a single flagellum. This does not include the time spent at the distal tip during conversion of anterograde trains to retrograde ones, which takes ~3.5–4 s (Fig. 5A; supplementary material Movie 9, comparable to the 2.5 s reported for *Chlamydomonas* (Qin et al., 2007)) and is the equivalent of 3–4 anterograde trains or ~10 units. Hence the total number of units within a flagellum is estimated to be at ~47 (27 anterograde units+10 transiting at the tip+10 on the retrograde leg) and a full flagellum cycle is expected to last for ~18 s on average (between 16 to 22 s according to the initial rate of the anterograde train). Remarkably, recovery rate reaches a plateau exactly within this margin (Fig. 5B), suggesting that the majority of the fluorescent material that replenishes the flagellum base after bleaching is due to recycling of IFT trains coming back from the flagellum compartment.

If this assumption were correct, one would expect a correlation between the recovery time at the flagellum base and the time spent by IFT trains in the flagellum. We have seen above that IFT rates and speeds are increased when cells are maintained at 37°C and the FRAP experiments were reproduced in these conditions.

Table 2. Frequency of IFT trains in the GFP::IFT52 expressing strain

| T | Anterograde (A) | | Retrograde (R) | | Ratio R:A | |
	Proximal	Distal	Proximal	Distal	Proximal	Distal
27°C	0.89	0.86	2.48	2.47	2.78	2.87
37°C	1.02	0.98	3.31	3.30	3.24	3.37

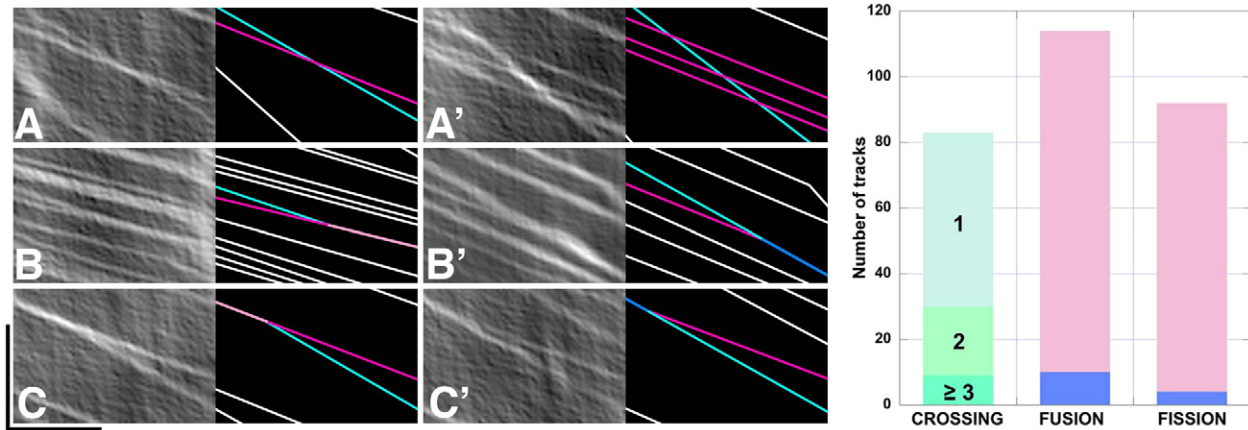Frequencies are given as number of trains per second.

Fig. 4. Anterograde trains interact in the same flagellum. (A–C) Kymographs (left panels) and schematic representation of traces of interest (right panels) where fast trains are shown in pink and slow trains are shown in blue. When a fast train catches up a slow one, three situations are observed. Quantification of each scenario is shown in **D**. First, a fast train overtakes one (A) ('1' in D) or more (A′) ('2' or '≥3' in D) slow trains, resulting in crossings on the kymographs. Second, a fast train catches up a slow one, fuses with it and the couple continues either at the fast rate (B) (light pink in D) or at the slow rate (B′) (dark blue in D). Third, fission events correspond to a fast train splitting into a fast and a slow train (C) (pink in D), or to a slow train splitting into a fast and slow train (C′) (blue on D). Data were compiled from 16 movies including a total of 715 trains. All kymographs are shown at the same magnification. Scale bars: horizontal, 5 µm; vertical, 5 s.

Total running time is now expected to be between 10 and 13 s for trains having travelled at the fast and the slow velocity during the anterograde part of the journey. FRAP analysis showed that the dwell time at the distal end was only 1 s, leading to 11 to 14 s to complete a cycle. A total of 22 cells could be analysed and the averaged data are presented at Fig. 5D (see supplementary material Movie 11 for an example of an individual cell). The rate of recovery was 45%, similar to what had been observed at 27℃, but the speed of recovery was faster reaching a peak at 12 s, exactly within the predicted margin.

To further support the view that the time spent in the flagellum dictates fluorescence recovery at the flagellum base, a correlation should also exist with the flagellum length. This can be addressed in cells assembling a new flagellum whose length varies according to the stage of the cell cycle (Robinson et al., 1995). Two examples are presented (Fig. 5E; supplementary material Movie 12), where the cell has duplicated its basal bodies that are both positive for GFP::IFT52 and is constructing a new flagellum whose length has reached ∼8 µm. Bleaching the fluorescent signal exclusively at the base of the new flagellum resulted in the same cascade of events that was observed for cells with a single flagellum: loss of new fluorescent anterograde trains, continued motion of the fluorescent anterograde and retrograde trains present within the flagellum before bleaching, return of retrograde trains to the base that progressively recovers fluorescent material and emergence of new fluorescent anterograde particles (Fig. 5E; supplementary material Movie 12). Fluorescence recovery at the flagellum base reached 40 to 50%, in the same range as observed for uni-flagellated cells. However, the time elapsed was ∼8–10 s, i.e. much faster compared to cells with a full-length flagellum and in agreement with the calculated time of recovery based on recycling of fluorescent proteins coming from a shorter flagellum. This experiment was reproduced on cells with a new flagellum of various lengths revealing a clear tendency towards shorter recovery times in shorter flagella (data not shown). An averaging analysis cannot be produced here since all these new flagella displayed different lengths. Overall, these results obtained in three different situations demonstrate active exchange of GFP::IFT52 protein between the flagellum base and the flagellar compartment in trypanosomes, with a dependence on flagellum length and IFT velocity.

With all these data in hand, the rate of recovery at the flagellum base can be analysed by mathematical modelling based on a recycling concept where the content of returning IFT trains is mixed with the proteins present in the flagellum base pool, without a contribution of the cell body pool. The simplest model proposes that all the IFT protein stock found at the flagellum base is mobilised to participate to IFT in the flagellum (Fig. 5F). The best fit obtained for this model requires the presence of 90 units at the flagellum base (85 at 37℃). However, the shape of the curve of such a fit (red, Fig. 5B,D) does not match that of the experimental data (black, Fig. 5B,D). The shape of the recovery curve indicates that a faster replenishment of the flagellum base takes place. This can be explained if one considers that only a restricted fraction of the IFT proteins normally present at the flagellum base are able to penetrate the flagellum and contribute to IFT (Fig. 5G). The best fit for this model is reached when the total number of trains at the flagellum base is set to 45 (or 30 at 37℃) and when only 45% (42% at 37℃) of them, corresponding to 20 (13 at 37℃), are actively recycled to the flagellum to contribute to new anterograde trains (Fig. 5B,C, blue curves). In a pure queuing system where the 47 fluorescent units that are back from the flagellum accumulate at the flagellum base before re-entering the flagellum, they would represent 46% of the initial pool, so a maximum number of 102 units. This is quite close to the value predicted by the first model. However, the predicted dwell time at the flagellum base in this model should be ∼90/2.7 or 33 s, which is more than three times higher than the experimental value of ∼9 s. Even if some mixing between bleached and unbleached IFT proteins takes place at the
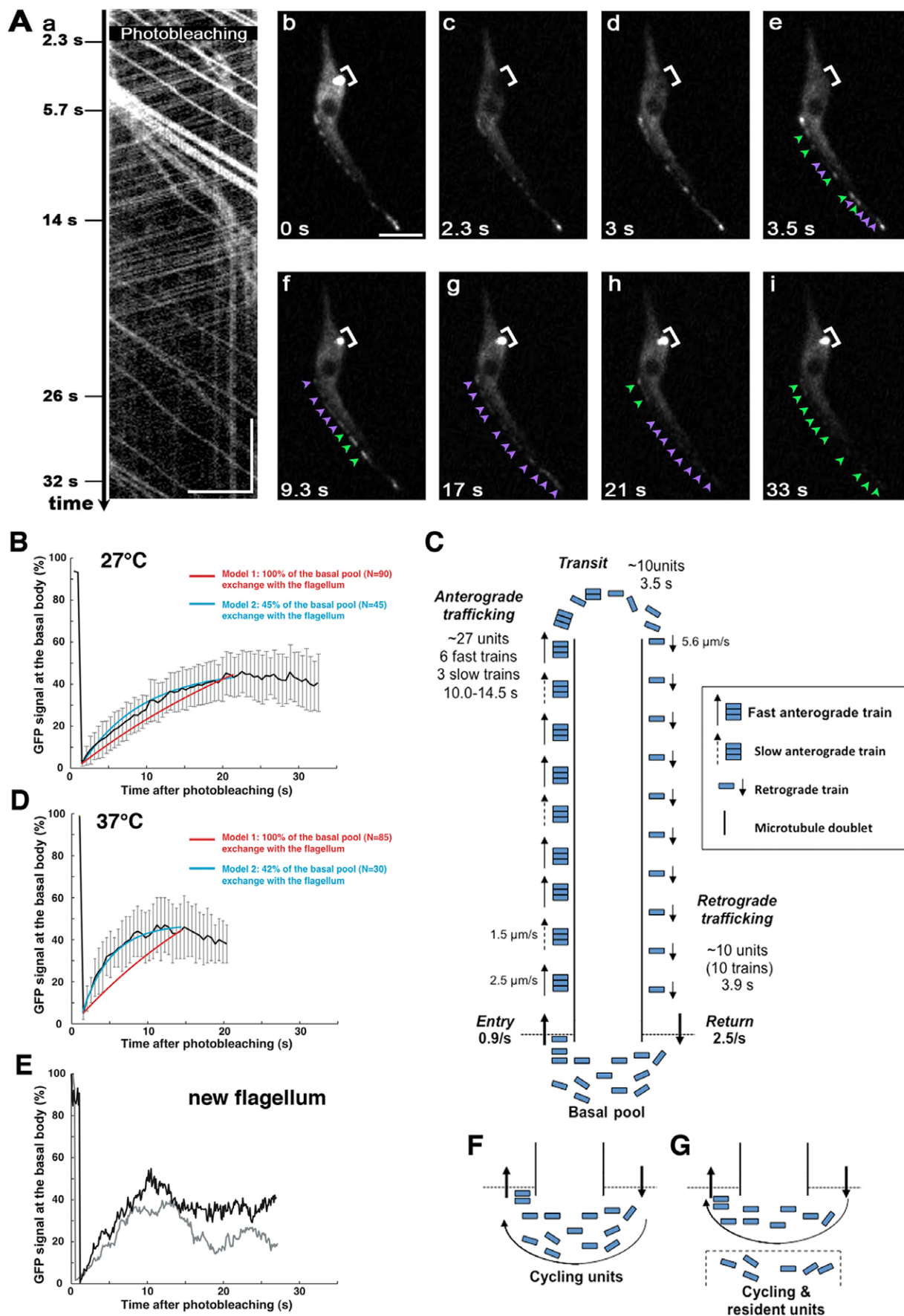
Fig. 5. See next page for legend.

Table 3. IFT parameters in various cell types

Species	Length	A (μm)	R (μm s^{-1})	R:A (μm s^{-1})	IFT cycle (s^{-1})	References
T. brucei (27℃)	22.3	2.4 (1.5)*	5.6	2.87	13.2 (18.4)*	This work
(37℃)	22.3	3.2 (2.2)*	7.4	3.37	9.9 (13.0)*	This work
C. reinhardtii (DIC)	12	1.8	3.1	1.25	10.5	(Iomini et al., 2001)
	12	1.9	2.8	1.07	10.6	(Dentler, 2005)
(IFT27::GFP)	12	2.3	nd	nd	nd	(Engel et al., 2009)
(IFT20::GFP)	12	2.1	2.5	nd	10.5	(Lechtreck et al., 2009)
C. elegans (middle)	4	0.7	1.2	nd	13.0[a]	(Snow et al., 2004)
(distal)	2.5	1.3	1.1	nd		(Snow et al., 2004)
LLC-PK1	3	0.6	0.7	nd	10.0	(Follit et al., 2006)
IMCD	6	0.4	0.6	nd	26.5	(Tran et al., 2008)
	6	0.3	0.6	nd	30.0	(Besschetnova et al., 2009)

A, anterograde transport; nd, not done; R, retrograde transport; *numbers in parentheses represent slow trains.
[a]cycle calculated as the sum of the time spent in the middle and distal segments.

flagellum base, this value is way too distant to explain the experimental data. In contrast, the prediction of 20 recycling units (45% of the 45 flagellum base units) produced by the model implying cycling and resident IFT proteins is matching quite closely the experimental data, providing further support for this model.

Discussion
IFT in the trypanosome flagellum
This study is the first quantitative report of IFT in the trypanosome model. We developed a robust method to quantify IFT that should be useful for the study of IFT in any organisms. It

Fig. 5. Dynamics of IFT at the flagellum base and in the flagellum.
(**A**) The fluorescent GFP::IFT52 signal at the flagellum base of cells possessing a single flagellum was bleached by a brief laser pulse restricted to the region of interest indicated in panel b. The signal intensity at the flagellum base is saturated but IFT trains in the flagellum are clearly visible (supplementary material Movie 9). Events were monitored in the flagellum using kymograph analysis (a) and in the whole cell by analysis of still images (b–i, supplementary material Movie 9). Please note that in this cell, the proximal part of the flagellum cannot be analysed since it is obscured by the cell body, resulting in a shift in timing of events between the flagellum and its base. (b) Image before photo-bleaching. (c) Immediately after bleaching, no signal is detected at the flagellum base but also at the flanking cytoplasmic region, a pool that is rapidly recovered (d–**e**). Both anterograde (green arrowheads) and retrograde (violet arrowhead) trains are detected in the flagellum (b–e). (f) New anterograde trains are not detected any more and the ones already present progressively reach the distal tip. (g) Only retrograde trains are detected. (h) New anterograde fluorescent trains appear at the proximal part of the flagellum. (i) Most retrograde fluorescent trains have gone back to the flagellum base area and new anterograde trains are reaching the tip of the flagellum. Notice the reduced fluorescent intensity of these trains, also visible on the kymograph (a, compare with kymographs presented in Figs 2, 3). Scale bar is 5 μm and time scale for the kymograph is 5 s. (**B**) Quantification of the fluorescent signal at the flagellum base before and after bleaching in cells where the fluorescence intensity at the flagellum base is not saturated. Recovery data were averaged from 10 separate movies. (**C**) Model showing the distribution of IFT trains in the flagellum. Fusion and fission events are not shown for the sake of clarity. (**D**) FRAP experiment with cells maintained at 37℃ (*n*=22 cells). (**E**) FRAP experiment at 27℃ in cells that possess two flagella, where only the base of the new flagellum was bleached (supplementary material Movie 11). Results for two distinct cells are presented. Recovery is faster when the flagellum is shorter. (**F**,**G**) Two models for IFT dynamics at the flagellum base, with involvement of all proteins in IFT (Model 1, red) or of only a limited pool (Model 2, blue).
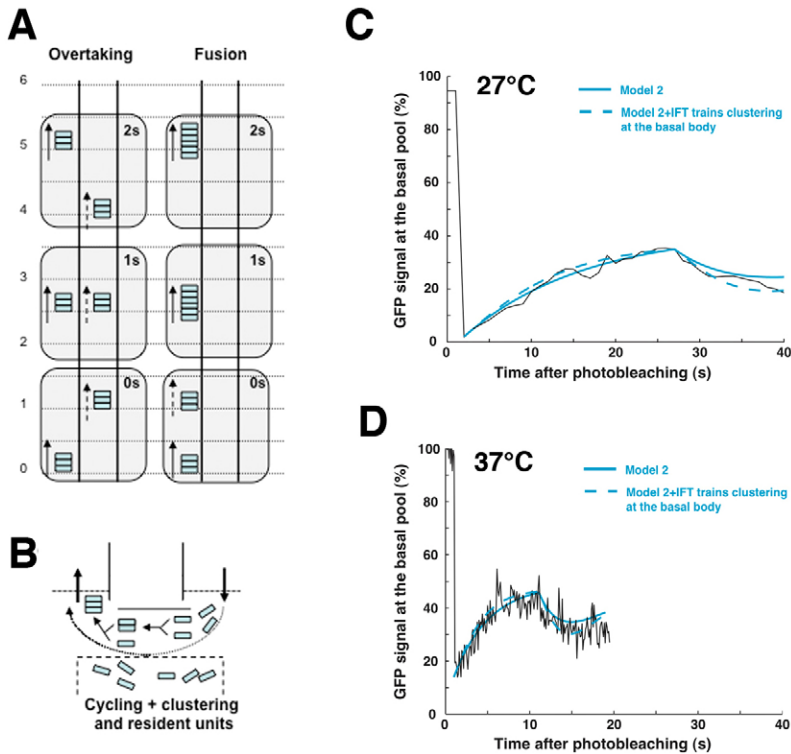
unravelled the fastest IFT speed reported so far, especially for retrograde transport (Table 3). By comparing IFT data from multiple systems, we noticed a tendency for faster IFT in longer flagella (Table 3), a fact that is supported by the progressive increase in IFT (Engel et al., 2009; Dentler, 2005) during flagellar regeneration in *Chlamydomonas* or by faster anterograde IFT in IMCD cells incubated with compounds that trigger elongation of the primary cilium (Besschetnova et al., 2009). It should be noted that the predicted elapsed time for a complete IFT cycle is quite similar in all systems reported so far (10–13 s), with the noticeable exception of primary cilia in IMCD cells (Table 3). However, this does not take into account the dwelling time spent at the distal tip during conversion of anterograde to retrograde trains.

The frequency of both anterograde and retrograde IFT trafficking had so far only been reported for *Chlamydomonas* using DIC approach and suggested a ratio close to 1:1 between anterograde and retrograde transport (Iomini et al., 2001; Dentler, 2005) (Table 3). These data are not in agreement with electron microscopy tomography studies that showed a 3-fold shorter length for IFT retrograde trains compared to anterograde ones (Pigino et al., 2009). This conundrum might be solved by our results that reveal, albeit in a different species, that anterograde trains are split in three at the distal tip. This appears more compatible with the structural analysis and suggests that the DIC approach does not detect all the IFT retrograde trains (Engel et al., 2009), possibly due to their smaller size. An alternate hypothesis could be the compaction of IFT proteins in tighter complexes but in this case retrograde trains should be brighter, which is not the case neither in trypanosomes nor in *Chlamydomonas* (Engel et al., 2009; Lechtreck et al., 2009). Finally, one could imagine that some IFT material is destroyed at the distal tip of the flagellum, for example by protease digestion. However, we found that close to 80% of the fluorescent signal carried by the anterograde trains is present in retrograde trains. This value is probably underestimated because retrograde trains are more likely to be undetected due to their smaller size and faster velocity.

The influence of temperature on IFT speed and frequency could be significant for the trypanosome life cycle. Indeed, a drop in temperature is one of the two key signals that triggers the differentiation from the bloodstream to the procyclic stage in the tsetse fly (Engstler and Boshart, 2004), resulting in the redistribution of a surface transporter involved in cis-aconitate entry, the other signal necessary for differentiation (Dean et al., 2009). The trypanosome flagellum has been proposed to work as a sensing

Fig. 6. Models for IFT trafficking in the flagellum and for recycling at the flagellum base. (**A**) If two trains travel on separate axonemal microtubule doublets, fast ones can overtake slow ones (left). If they travel on the same doublet, fast ones can fuse with slow ones (right). The box marked 0 s indicates the initial situation with a fast train catching up to a slow one and their expected positions are indicated after 1 and 2 s, the scale indicates the number of μm ran along the doublets.
(**B**) Clustering model for IFT recycling at the flagellum base.
(**C**) Individual sequence of fluorescence recovery at the flagellum base at 27℃ with models shown in Fig. 5G (solid blue lines) or Fig. 6B (dotted blue lines). (**D**) Same as C but for a cell incubated at 37℃.

element (Rotureau et al., 2009) and a possible reduction of IFT speed due to the temperature drop could be involved in modified exchange of signalling molecules between the flagellum and cell body compartments, comparable to what has been suggested for hedgehog function at the primary cilium (Scholey and Anderson, 2006). The increase in IFT at 37℃ could be explained by modifications in membrane fluidity and/or motor processivity.

Interaction of IFT anterograde trains within the flagellum

The discovery of two distinct motilities for anterograde IFT in the same flagellum is different from the *C. elegans* situation where two different velocities have been reported but on separate segments of the cilia (Snow et al., 2004). The fact that both overtaking and apparent fusion events (although this could not be shown formally given the current resolution limit) are observed indicates that trains can travel independently or can be restricted to the same doublet (Fig. 6A). However, the ratio of fusion versus overtaking events (1.2:1) is much higher than would be expected if the nine doublets were used stochastically. This supports the view that IFT trains are found on a restricted set of microtubules, as observed after chemical fixation and transmission electron microscopy analysis (Absalon et al., 2008). This is not simply due to the presence of the paraflagellar rod that is connected to the axoneme at the level of doublets 4 to 7, hence restricting the number of available doublets. Indeed, IFT particles are only encountered at doublets 3–4 and 7–8 whereas doublets 1, 2 and 9 are freely available. It also raises the question about how trains select these microtubules. One hypothesis could be that each doublet has its own molecular identity providing optimal ground for a specific type of molecular motor or of IFT trains. This identity could be derived from the flagellum base where, at least in some protists, each triplet can be structurally identified (Beisson and Wright, 2003) and therefore

could define the molecular identity to be transmitted to the axoneme microtubule. More simply, the selection could be made at the level of the flagellum base without requiring a specific molecular identity at the axoneme level.

The fate of IFT trains after their trip in the flagellum

Several hypotheses can be suggested to explain what happens to IFT train components once they have completed their trip in the flagellum. First, they could be destroyed upon flagellum exit and replaced by fresh IFT proteins. Second, trains could be directly recycled to the flagellar compartment without exchange with the flagellum base material. Third, returning trains could have to queue behind the proteins already present at the flagellum base, for example before conversion to anterograde trains. Fourth, proteins from returning trains could be mixed with the flagellum base pool and recruited to make new trains. The first two models can be discarded because they imply that recovery of the fluorescent signal at the flagellum base in our FRAP experiments should be independent of the time IFT trains spent in the flagellum. The absence of fluorescent anterograde trains penetrating the flagellum for at least 9 s following bleaching does not support the direct recycling model but is rather indicative of a queuing or a mixing model. However, the queuing model is not valid either because these new fluorescent trains are less bright than the original ones.

Our mathematical analysis integrating all experimental data reveals that the recovery of fluorescent signal at the flagellum base following photobleaching can be fully explained by material coming back from the flagellum using a minimum number of parameters. Nevertheless, preliminary RNAi experiments indicate a weak contribution of IFT proteins from the cytoplasmic pool to the flagellum base but with a slow kinetic

of exchange lasting 6 to 8 hours (our unpublished data). This contribution is probably negligible in the experimental conditions used here where incubations lasted 30 sec to a few minutes. The analysis supports a model where two pools of IFT proteins are present at the flagellum base. One of them is actively engaged in IFT and exchanges with material coming back from the flagellum whereas the other one has no or much slower dynamics. These 'resident' IFT proteins may play other functions, as suggested in mammalian cells where IFT88 has been shown to participate to the control of the cell cycle or to the positioning of the mitotic spindle (Robert et al., 2007; Delaval et al., 2011). Treatment of trypanosomes with detergent revealed that most of the IFT proteins are found in the soluble fraction, in agreement with proteins undergoing rapid movement. However, a small proportion was consistently detected in the cytoskeletal fraction and localised at the flagellum base (Absalon et al., 2008; Adhiambo et al., 2009).

The mixing model predicts that the total amount of fluorescence at the flagellum base should decrease after having reached the peak because of the return of the non-fluorescent trains that penetrated the flagellum immediately after the bleach (Fig. 5A). Indeed, a clear decrease is detected on multiple individual films (6/10 at 27°C and 21/30 at 37°C) but at slightly shifted times. However, averaging all the sequences tended to dim the later part of the curve, restricting the analysis (Fig. 5B,D). We therefore ran the mixing model (blue curve on Fig. 5B,D) on two individual films taken at either 27°C (Fig. 6B) or 37°C (Fig. 6C). Careful examination of events past the plateau observed at 22 s (27°C) or 12 s (37°C) uncovered close fitting of the experimental data also in this part of the curve. The model can still be refined by the inclusion of a clustering condition, in order to take into account the necessary conversion of IFT retrograde trains to anterograde trains for the next cycle. This could require several steps, such as disassembly of the retrograde train, release of the dynein motor, formation of the anterograde train and association to the kinesin motor. We considered two steps in the model (since at least three units are required to constitute an anterograde train, Fig. 6D) and that provided an even more precise fit of the experimental data (Fig. 6B,C, dotted curves).

Materials and Methods

Trypanosome cell lines and cultures
All cells used for this work were derivatives of *T. brucei* strain 427 (procyclic stage) and were cultured in SDM79 medium supplemented with hemin and 10% foetal calf serum. The cell lines expressing GFP::IFT52 has been described elsewhere (Absalon et al., 2008). For expression of GFP::DHC2.1, the sequence encoding the first 777 nucleotides (1–777) was amplified by PCR from genomic DNA as template with the proof-reading enzyme Phusion^{TM} (Finnzyme), using GCATCAGCTAGCATGGTTTCGGCAGAGAAGG (NheI site underlined) as forward primer and CTAATCGGGATCCCTACTCGCTAGATTGGAG (*Bam*HI site underlined) as reverse primer. The PCR product was cloned in frame downstream of the *GFP* gene in the pPCPFR expression vector (Adhiambo et al., 2009) and verified by sequencing (Genome Express). The construct was linearised within the *DHC2.1* sequence with the enzyme MfeI and nucleofected (Burkard et al., 2007) in wild-type trypanosomes, leading to integration by homologous recombination in the endogenous locus and to expression of the full length coding sequence of DHC2.1 fused to GFP. This recombined gene is flanked by the 5′ untranslated region of the *PFR2* gene and by the 3′ untranslated region of *DHC2.1*. Expression of the fusion of appropriate size was confirmed by western blotting with an anti-GFP antibody (not shown).

Life microscopy analysis
The expression of GFP::IFT52 or GFP::DHC2.1 was first observed directly with a DMI4000 Leica microscope using mercury bulb for excitation. Images were captured with an exposure time of 150–400 ms with a Retiga-SRV camera (Q-Imaging). Images were analysed using the IPLab Spectrum 3.9 software

(Scanalytics & BD Biosciences) or ImageJ. For reduced acquisition time and for IFT quantification we used a Zeiss inverted microscope (Axiovert 200) equipped with an oil immersion objective (magnification×63 with a 1.4 numerical aperture) and a spinning disk confocal head (CSU22, Yokogawa). Images were acquired using Volocity software with an EMCCD camera (C-9100, Hamamatsu) operating in streaming mode. A sample of cell (a 100 μL drop) was taken directly from the culture grown at 6 to 8×10^6 cells mL^{-1} and trapped between slide and coverslip. The samples were kept at 27°C or 37°C using two different devices, a temperature controlled chamber and a fast response mini-stage temperature controller allowing rapid changes in temperatures. This device allows variation of the sample temperature between 4 and 38°C at rates of ~1°C s^{-1}, and provides long-term temperature stability within ±0.3°C based on Peltier element (Gorjánácz et al., 2007a; Gorjánácz et al., 2007b). The samples were used no longer than 30 minutes. 345 movies of GFP::IFT52 cells at 27°C were acquired in eight independent experiments, 100 movies in three experiments at 37°C and 129 movies at 27°C in four independent experiments for EGFP::DHC2.1 cells. Movies for in-depth analysis were taken out of six independent experiments for IFT52 at 27°C (40 movies), two at 37°C (20 movies) and three for DHC2.1 (10 movies).

Fluorescent recovery after photobleaching (FRAP) analysis
For FRAP experiments, cells were mounted between slide and coverslip and observed with same imaging conditions as described before. Time-lapse sequences were acquired to analyse GFP signal recovery after photo-bleaching. The presented movies are representative for both experiments (cells possessing just a single flagellum and cells presenting an old flagellum and a new in construction). For the experiments on cells presenting one flagellum, 96 image sequences were acquired in eight independent FRAP experiments. Movies were taken at maximum speed of acquisition (no time lapse). Exposure time was 100 ms per frame and the actual time between two frames was around 0.111 s and 0.116 s (binning was 1×1 pixels). For the experiments on cells presenting two flagella and where only the base of the new one was photo-bleached, 30 image sequences were acquired in seven independent FRAP experiments. Movies were taken at maximum speed of acquisition (no time lapse). Exposure time was 100 ms per frame and the actual time between two frames was around 0.111 s and 0.116 s (binning was 1×1 pixels).

Fluorescence intensity was measured in the region of interest using ImageJ software (for example the flagellum base). To normalise data, background was subtracted and overall photo-bleaching over time was normalised using another equivalent source of GFP (a flagellum base fluorescent protein pool in a cell that had not been bleached) for each individual image. This allows to correct GFP photobleaching due to laser exposure. Because of the large file size, the field of view has been restricted to cells of interest in the presented movie.

Kymograph extraction and analysis
In order to identify IFT particle trajectories through time we used the kymograph analysis (Piperno et al., 1998). Each line of the kymograph corresponds to the observed intensities of a given train during its trip in the flagellum, providing a very concise summary over an extended period of time. Our technique is based on a novel adaptive and directional band-pass filtering method that allows the separation of trails of opposite directions. The filtering method exploits the curvelet analysis of the kymograph image to automatically adapt to the trains characteristics and select oriented features (specific details available in Chenouard et al., 2010). In practice, the filtering parameters are adjusted such that artefacts (e.g. fluorescence coming from the trypanosome body) are compensated for, and two different directionality setups are chosen as to select anterograde or retrograde IFT particles respectively. For each separated kymograph, trajectories of IFT particles are built in an automated manner as to allow the analysis of large data sets. The automatic tracking method consists of two stages: (1) we identify putative particle positions by detecting a set of relevant local intensity maxima which are analysed to achieve a sub-pixel accuracy, (2) the set of positions are linked through time thanks to a statistical tracking algorithm which automatically discards wrong detections and compensates for missing detections thanks to particle motion modelling over multiple frames (Chenouard et al., 2009). Human inspection and correction is then performed to achieve optimal accuracy. Track correction is semi-automated as the operator only indicates extremities of missing particle trails in the kymograph image, while complete trajectories are estimated with a shortest path algorithm that automatically follows the trails between the identified extremities. We automatically extract several individual particle indicators as a function of time from the set of trajectories: the train length, its intensity averaged over the particle area, and its velocity. We also set some control points on the flagellum, count the number of particles crossing these gates, and estimate the frequency of these events. These measures are collected and eventually compared and averaged over multiple particles and individuals. The semi-automatic pipeline[1] allows the accurate extraction of a large number of trajectories from an image sequence comprised of several hundred frames within only few minutes, hence making possible the analysis of large data set and the computation of significant statistics. Indeed, we extract information such as train density, velocity, intensity and length. In the case of trains that changed speed during the anterograde leg, tracks were split as straight lines and the individual speed of these was measured. Pauses were rarely observed but very slow tracks were

consistently detected and grouped manually as a separate category. Due to their low proportion, these very slow trains are not detected in the BIC analysis.

IFT rate statistical analysis: the Bayesian information criterion (BIC)

Due to the large intrinsic variability of IFT velocities in each cell, BIC (Schwarz, 1978) is used to uncover the number of modes in both retrograde and anterograde IFT velocities. Indeed, modelling the empirical distribution $e(x)$ of IFT speeds with a weighted sum of Gaussian laws, the BIC permits to select the right number of laws to put in the model and to avoid overfitting, by introducing a penalty term for the number of parameters in the fitting model. More precisely, representing $e(x)$ with a Gaussian mixture model

$$e(x) = \sum_{i=1}^{p} \alpha_i N(\mu_i, \sigma_i)$$

where p is the number of Gaussian laws in the mixture, α_i the weight of each law and μ_i, σ_i the corresponding mean and variance, we first searched, for a fixed p, the optimal parameters $(\alpha_i^*, \mu_i^*, \sigma_i^*)_{1..p}$ that maximise the likelihood L of the model to data

$$L(\alpha_1, \mu_1, \sigma_1; ...; \alpha_p, \mu_p, \sigma_p) = \prod_{j=1}^{n} \left[\sum_{i=1}^{p} \frac{\alpha_i}{\sqrt{2\pi}\sigma_i} \exp\left(-(x_j - \mu_i)^2 / 2\sigma_i\right) \right]$$

where $(x_1, x_2, ..., x_n)$ are the observed retrograde (resp. anterograde) IFT rates in an individual cell and n the corresponding sample size. Consequently, this first step of the analysis provides the calibrated parameters $(\alpha_i^*, \mu_i^*, \sigma_i^*)_{1..p}$, when fitting a p-mixture model to data. Then, the optimal number of modes p^* accounting for retrograde or anterograde IFT rates was computed by minimising the BIC

$$BIC(p) = -2\log(L_p^*) + k_p \log(n)$$

where L_p^* is the maximised likelihood the p-mixture model:

$$L_p^* = \prod_{j=1}^{n} \left[\sum_{i=1}^{p} \frac{\alpha_i^*}{\sqrt{2\pi}\sigma_i^*} \exp\left(-(x_j - \mu_i^*)^2 / 2\sigma_i^*\right) \right]$$

and k_p is the number of free parameters (#$\{S\}$ denotes the cardinal of an ensemble S)

$$k_p = \#\{\mu_1, \sigma_1, \mu_2, \sigma_2, ..., \mu_p, \sigma_p, \alpha_1, \alpha_p, ..., \alpha_{p-1}\} = 3p - 1$$

Applying this analysis to the measured IFT rates, we found that the anterograde IFT was bimodal ($P^*=2$) in 29 of the 41 cells (71%; 13/18 EGFP::IFT52 cells at 27°C, 12/16 EGFP::IFT52 cells at 37°C and 4/7 EGFP::DHC2.1 cells).

Mean parameters:

$$\bar{\alpha}_1 = \frac{1}{m}\sum_{k=1}^{m} \alpha_1^*(k), \bar{\alpha}_2 = 1 - \bar{\alpha}_1, \ \bar{\mu}_1 = \frac{1}{m}\sum_{k=1}^{m} \mu_1^*(k), \bar{\mu}_2 = \frac{1}{m}\sum_{k=1}^{m} \mu_2^*(k)$$

are summarised in Table 1. $m=13$, 12 and 4 for EGFP::IFT52 (27°C), EGFP::IFT52 (37°C) and EGFP::DHC2.1, respectively, and .*(k) denotes the optimal parameter obtained for cell k.

Modelling the recycling of IFT proteins at the flagellum base

To analyse photobleaching experiments, we considered that the fluorescence recovery at time t, $\alpha(t)$ is entirely controlled by exchange of fluorescent material with the flagellum. In particular IFT fluorescent units enter the flagellum with effective frequency $\alpha(t).f$, where f is the anterograde trains frequency ($f\sim0.89*3=2.67$ IFT units per second at 27°C), to be further transported towards the distal tip. We considered that the fluorescence of IFT trains remained unchanged during their journey inside the flagellum, which lasts a mean time τ, and that $f.\alpha(t-\tau)$ fluorescent proteins consequently comes back to the flagellum base at the same time. Using the mean anterograde (v_a) and retrograde (v_r) IFT velocities that were measured experimentally (Table 1), the length $L=23$ μm of the flagellum and the mean lag time τ_{lag} (~4 s at 27°C and ~1 s at 37°C) of IFT proteins at the flagellum distal tip, the duration τ of the IFT flagellum trip can be estimated to:

$$\tau = \tau_{lag} + L\left(\frac{1}{v_a} + \frac{1}{v_r}\right)$$

Consequently, the fluorescence recovery rate $\alpha(t)$ is the solution of the dynamical equation:

$$\frac{d\alpha(t)}{dt} = \frac{1}{N}f(\alpha(t-\tau) - \alpha(t)) \tag{1}$$

where N is the total number of IFT proteins in the flagellum base exchanging with the flagellum. For $0<t<\tau$, only pure fluorescent particles, that were into the

flagellum when photobleaching of the flagellum base occurred, are coming back to the flagellum base and dynamic equation (1) reduces to:

$$\frac{d\alpha(t)}{dt} = \frac{1}{N}f(1 - \alpha(t))$$

Finally, if we consider that N represents only a restricted fraction of the total number N_T of flagellum base IFT proteins, that are able to penetrate the flagellum and contribute to IFT, the fluorescence recovery is then equal to $N/N_T \ \alpha(t)$.

Integrating the clustering of IFT units at the flagellum base

To account for the necessary conversion of IFT retrograde trains to anterograde trains for the next cycle, we decided to further include a clustering condition of IFT proteins at the flagellum base to our previous model. Because retrograde IFT trains that are coming back to the flagellum base cluster into novel trains that contain three individual units before returning into the flagellum, we considered that the flagellum base pool N of IFT proteins that exchange with the flagellum can be divided into three subpopulations: $N=N_1+N_2+N_3$, where N_1 is the number of single IFT units that are coming back from the flagellum, N_2 the number of IFT units that are engaged into intermediate clusters of two units and N_3 the number of units engaged in final clusters of three units. These 3-cluster units are then able to re-enter the flagellum as anterograde IFT trains. The fluorescence recovery $\alpha(t)$ after photobleaching is thus equal to:

$$\alpha(t) = \frac{\alpha_1(t)N_1 + \alpha_2(t)N_2 + \alpha_3(t)N_3}{N}$$

where $\alpha_1(t)$, $\alpha_2(t)$ and $\alpha_3(t)$ are the proportion of fluorescent proteins that are respectively engaged in single IFT units, and in 2- and 3-clusters.

Moreover, we assumed that the binding rate k between single IFT units or between a single unit and a 2-cluster are equal. Consequently, a single fluorescent unit can bind to another single unit with rate $k.N_1.N_1$, or it can bind to a 2-cluster with rate $k.N_1.N_2/2$, where $N_2/2$ is the effective number of 2-clusters inside the flagellum base. Then, if the two single IFT units that bind to form a 2-cluster are both fluorescent, with a probability $\alpha_1^2(t)$, the pool of fluorescent single IFT units is depleted by two units that are transferred into the 2-cluster pool. While if only one single IFT unit is fluorescent, with probability $2\alpha_1(t)(1-\alpha_1(t))$, the single units pool is only depleted by one unit. Because a fluorescent single unit can also bind a 2-cluster, we finally obtain the dynamical equation

$$\frac{d\alpha_1(t)}{dt} = \frac{1}{N_1}\left(f\alpha_3(t-\tau) - \frac{kN1N2}{2}\alpha_1(t) - kN_1^2\left(2\alpha_1^2(t) + 2\alpha_1(t)(1-\alpha_1(t))\right)\right)$$

which reduces to

$$\frac{d\alpha_1(t)}{dt} = \frac{1}{N_1}\left(f\alpha_3(t-\tau) - \frac{kN1N2}{2}\alpha_1(t) - 2kN_1^2\alpha_1(t)\right)$$

where $f\alpha_3(t-\tau)$ is the effective number of fluorescent proteins that enters the flagellum at time $t-\tau$, and come back at the flagellum base after their flagellum journey which lasts τ. In a same way, dynamical equation for $\alpha_2(t)$ and $\alpha_3(t)$ reads

$$\frac{d\alpha_2(t)}{dt} = \frac{1}{N_2}\left(2\alpha_1(t)kN_1^2 - kN1N2\alpha_2(t)\right) \text{ and}$$

$$\frac{d\alpha_3(t)}{dt} = \frac{1}{N_3}\left(k\frac{N_1N_2}{2}(2\alpha_2(t) + \alpha_1(t)) - f\alpha_3(t)\right)$$

Before photobleaching, all the IFT particles of the flagellum base are fluorescent: $\alpha_i(t)=1$ for $i=1$, 2 and 3, and $\frac{d\alpha_i(t)}{dt}=0$. Re-injecting these initial conditions in previous dynamical equations, we obtain the relations $N_2=2N_1$, and $N_1 = \sqrt{f/3k}$. The model is not very sensitive to the binding constant k that was arbitrarily set at $k = \frac{25f}{3N^2}$, which is equivalent to the stoichiometry condition $N_2=N_3=2N_1$.

Supplementary material available online at
http://jcs.biologists.org/lookup/suppl/doi:10.1242/jcs.117069/-/DC1

References

Absalon, S., Blisnick, T., Kohl, L., Toutirais, G., Doré, G., Julkowska, D., Tavenet, A. and Bastin, P. (2008). Intraflagellar transport and functional analysis of genes required for flagellum formation in trypanosomes. *Mol. Biol. Cell* **19**, 929-944.

Adhiambo, C., Blisnick, T., Toutirais, G., Delannoy, E. and Bastin, P. (2009). A novel function for the atypical small G protein Rab-like 5 in the assembly of the trypanosome flagellum. *J. Cell Sci.* **122**, 834-841.

Beisson, J. and Wright, M. (2003). Basal body/centriole assembly and continuity. *Curr. Opin. Cell Biol.* **15**, 96-104.

Besschetnova, T. Y., Roy, B. and Shah, J. V. (2009). Imaging intraflagellar transport in mammalian primary cilia. *Methods Cell Biol.* **93**, 331-346.

Brown, J. M., Marsala, C., Kosoy, R. and Gaertig, J. (1999). Kinesin-II is preferentially targeted to assembling cilia and is required for ciliogenesis and normal cytokinesis in Tetrahymena. *Mol. Biol. Cell* **10**, 3081-3096.

Burkard, G., Fragoso, C. M. and Roditi, I. (2007). Highly efficient stable transformation of bloodstream forms of Trypanosoma brucei. *Mol. Biochem. Parasitol.* **153**, 220-223.

Chenouard, N., Bloch, I. and Olivo-Marin, J. C. (2009). *Multiple Hypothesis Tracking in Microscopy Images*. 6th IEEE International Symposium on BioImaging, ISBI 2009, Boston, USA, 2009.

Chenouard, N., Buisson, J., Bloch, I., Bastin, P. and Olivo-Marin, J. C. (2010). *Curvelet Analysis of Kymograph for Tracking Bi-directional Particles in Flurescence Microscopy Images*. 17th IEEE International Conference on Image Processing, ICIP 2010, Hong Kong, China, 2010.

Cole, D. G., Diener, D. R., Himelblau, A. L., Beech, P. L., Fuster, J. C. and Rosenbaum, J. L. (1998). Chlamydomonas kinesin-II-dependent intraflagellar transport (IFT): IFT particles contain proteins required for ciliary assembly in *Caenorhabditis elegans* sensory neurons. *J. Cell Biol.* **141**, 993-1008.

Dean, S., Marchetti, R., Kirk, K. and Matthews, K. R. (2009). A surface transporter family conveys the trypanosome differentiation signal. *Nature* **459**, 213-217.

Delaval, B., Bright, A., Lawson, N. D. and Doxsey, S. (2011). The cilia protein IFT88 is required for spindle orientation in mitosis. *Nat. Cell Biol.* **13**, 461-468.

Dentler, W. (2005). Intraflagellar transport (IFT) during assembly and disassembly of Chlamydomonas flagella. *J. Cell Biol.* **170**, 649-659.

Engel, B. D., Ludington, W. B. and Marshall, W. F. (2009). Intraflagellar transport particle size scales inversely with flagellar length: revisiting the balance-point length control model. *J. Cell Biol.* **187**, 81-89.

Engstler, M. and Boshart, M. (2004). Cold shock and regulation of surface protein trafficking convey sensitization to inducers of stage differentiation in Trypanosoma brucei. *Genes Dev.* **18**, 2798-2811.

Follit, J. A., Tuft, R. A., Fogarty, K. E. and Pazour, G. J. (2006). The intraflagellar transport protein IFT20 is associated with the Golgi complex and is required for cilia assembly. *Mol. Biol. Cell* **17**, 3781-3792.

Gorjánácz, M., Klerkx, E. P., Galy, V., Santarella, R., López-Iglesias, C., Askjaer, P. and Mattaj, I. W. (2007a). *Caenorhabditis elegans* BAF-1 and its kinase VRK-1 participate directly in post-mitotic nuclear envelope assembly. *EMBO J.* **26**, 132-143.

Gorjánácz, M., Mattaj, I. W. and Rietdorf, J. (2007b). Some like it hot: switching biology on the microscope. *Imaging Micro.* **9**, 26-27.

Hao, L. and Scholey, J. M. (2009). Intraflagellar transport at a glance. *J. Cell Sci.* **122**, 889-892.

Huangfu, D., Liu, A., Rakeman, A. S., Murcia, N. S., Niswander, L. and Anderson, K. V. (2003). Hedgehog signalling in the mouse requires intraflagellar transport proteins. *Nature* **426**, 83-87.

Iomini, C., Babaev-Khaimov, V., Sassaroli, M. and Piperno, G. (2001). Protein particles in Chlamydomonas flagella undergo a transport cycle consisting of four phases. *J. Cell Biol.* **153**, 13-24.

Julkowska, D. and Bastin, P. (2009). Tools for analyzing intraflagellar transport in trypanosomes. *Methods Cell Biol.* **93**, 59-80.

Kohl, L., Robinson, D. and Bastin, P. (2003). Novel roles for the flagellum in cell morphogenesis and cytokinesis of trypanosomes. *EMBO J.* **22**, 5336-5346.

Kozminski, K. G., Johnson, K. A., Forscher, P. and Rosenbaum, J. L. (1993). A motility in the eukaryotic flagellum unrelated to flagellar beating. *Proc. Natl. Acad. Sci. USA* **90**, 5519-5523.

Kozminski, K. G., Beech, P. L. and Rosenbaum, J. L. (1995). The *Chlamydomonas* kinesin-like protein FLA10 is involved in motility associated with the flagellar membrane. *J. Cell Biol.* **131**, 1517-1527.

Lechtreck, K. F., Johnson, E. C., Sakai, T., Cochran, D., Ballif, B. A., Rush, J., Pazour, G. J., Ikebe, M. and Witman, G. B. (2009). The Chlamydomonas reinhardtii BBSome is an IFT cargo required for export of specific signaling proteins from flagella. *J. Cell Biol.* **187**, 1117-1132.

Morsci, N. S. and Barr, M. M. (2011). Kinesin-3 KLP-6 regulates intraflagellar transport in male-specific cilia of *Caenorhabditis elegans*. *Curr. Biol.* **21**, 1239-1244.

Orozco, J. T., Wedaman, K. P., Signor, D., Brown, H., Rose, L. and Scholey, J. M. (1999). Movement of motor and cargo along cilia. *Nature* **398**, 674.

Pazour, G. J., Dickert, B. L., Vucica, Y., Seeley, E. S., Rosenbaum, J. L., Witman, G. B. and Cole, D. G. (2000). *Chlamydomonas* IFT88 and its mouse homologue, polycystic kidney disease gene tg737, are required for assembly of cilia and flagella. *J. Cell Biol.* **151**, 709-718.

Pigino, G., Geimer, S., Lanzavecchia, S., Paccagnini, E., Cantele, F., Diener, D. R., Rosenbaum, J. L. and Lupetti, P. (2009). Electron-tomographic analysis of intraflagellar transport particle trains *in situ*. *J. Cell Biol.* **187**, 135-148.

Piperno, G., Siuda, E., Henderson, S., Segil, M., Vaananen, H. and Sassaroli, M. (1998). Distinct mutants of retrograde intraflagellar transport (IFT) share similar morphological and molecular defects. *J. Cell Biol.* **143**, 1591-1601.

Qin, H., Wang, Z., Diener, D. and Rosenbaum, J. (2007). Intraflagellar transport protein 27 is a small G protein involved in cell-cycle control. *Curr. Biol.* **17**, 193-202.

Robert, A., Margall-Ducos, G., Guidotti, J. E., Brégerie, O., Celati, C., Bréchot, C. and Desdouets, C. (2007). The intraflagellar transport component IFT88/polaris is a centrosomal protein regulating G1-S transition in non-ciliated cells. *J. Cell Sci.* **120**, 628-637.

Robinson, D. R., Sherwin, T., Ploubidou, A., Byard, E. H. and Gull, K. (1995). Microtubule polarity and dynamics in the control of organelle positioning, segregation, and cytokinesis in the trypanosome cell cycle. *J. Cell Biol.* **128**, 1163-1172.

Rompolas, P., Pedersen, L. B., Patel-King, R. S. and King, S. M. (2007). Chlamydomonas FAP133 is a dynein intermediate chain associated with the retrograde intraflagellar transport motor. *J. Cell Sci.* **120**, 3653-3665.

Rotureau, B., Morales, M. A., Bastin, P. and Späth, G. F. (2009). The flagellum-mitogen-activated protein kinase connection in Trypanosomatids: a key sensory role in parasite signalling and development? *Cell. Microbiol.* **11**, 710-718.

Scholey, J. M. and Anderson, K. V. (2006). Intraflagellar transport and cilium-based signaling. *Cell* **125**, 439-442.

Schwarz, G. (1978). Estimating the dimension of a model. *Ann. Stat.* **6**, 461-464.

Signor, D., Wedaman, K. P., Orozco, J. T., Dwyer, N. D., Bargmann, C. I., Rose, L. S. and Scholey, J. M. (1999). Role of a class DHC1b dynein in retrograde transport of IFT motors and IFT raft particles along cilia, but not dendrites, in chemosensory neurons of living *Caenorhabditis elegans*. *J. Cell Biol.* **147**, 519-530.

Snow, J. J., Ou, G., Gunnarson, A. L., Walker, M. R., Zhou, H. M., Brust-Mascher, I. and Scholey, J. M. (2004). Two anterograde intraflagellar transport motors cooperate to build sensory cilia on C. elegans neurons. *Nat. Cell Biol.* **6**, 1109-1113.

Tran, P. V., Haycraft, C. J., Besschetnova, T. Y., Turbe-Doan, A., Stottmann, R. W., Herron, B. J., Chesebro, A. L., Qiu, H., Scherz, P. J., Shah, J. V. et al. (2008). THM1 negatively modulates mouse sonic hedgehog signal transduction and affects retrograde intraflagellar transport in cilia. *Nat. Genet.* **40**, 403-410.